Nanoscale

Accepted Manuscript

This article can be cited before page numbers have been issued, to do this please use: C. Boutopoulos, A. Degallier, M. Sansone, A. Blanchard-Dionne, É. Lecavalier-Hurtubise, É. Boulais and M. Meunier, *Nanoscale*, 2016, DOI: 10.1039/C6NR03888C.

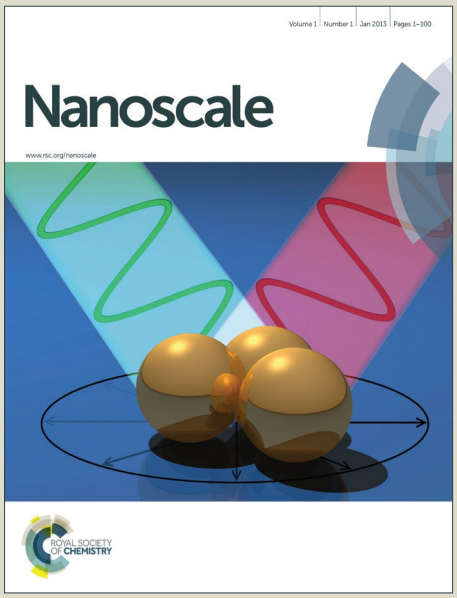

ROYAL SOCIETY OF CHEMISTRY

www.rsc.org/nanoscale

Nanoscale

View Article Online
DOI: 10.1039/C6NR03888C

ARTICLE

Photon-induced generation and spatial control of extreme pressure at the nanoscale with a gold bowtie nano-antenna platform

Received 00th January 20xx,
Accepted 00th January 20xx

DOI: 10.1039/x0xx00000x

www.rsc.org/

Christos Boutopoulos[a,b], Adrien Dagallier[a], Maria Sansone[a,c], Andre-Pierre Blanchard-Dionne[a], Évelyne Lecavalier-Hurtubise[1], Étienne Boulais[a,d], Michel Meunier[a*]

Precise spatial and temporal control of pressure stimulation at the nanometer scale is essential for the fabrication and manipulation of nano-objects, and for exploring single-molecule behaviour of matter under extreme conditions. However, state-of-the-art nano-mechanical transducers require sophisticated driving hardware and are currently limited to moderate pressure regimes. Here we report a gold plasmonic bowtie (AuBT) nano-antennas array that can generate extreme pressure stimulus of ~100 GPa in the ps (10^{-12} s) time scale with sub-wavelength resolution upon irradiation with ultra-short laser pulses. Our method leverages the non-linear interaction of photons with water molecules to excite a nano-plasma in the plasmon-enhanced near-field and induce extreme thermodynamic states. The proposed method utilizes laser pulses, which in contrast to micro- and nano-mechanical actuators offers simplicity and versatility. We present time-resolved shadowgraphic imaging, electron microscopy and simulation data that suggest that our platform can efficiently create cavitation nano-bubbles and generate intense pressure in specific patterns, which can be controlled by the selective excitation of plasmon modes of distinct polarizations. This novel platform should enable probing non-invasively the mechanical response of cells and single-molecules at time and pressure regimes that are currently difficult to reach with other methods

Introduction

Photons are unique vectors of energy and momentum that can be precisely directed and delivered to interact mechanically with micro and nano-sized objects. For instance, optical tweezers[1] are capable of trapping dielectric objects via light-induced forces, providing unique opportunities for cell manipulation in biological research. The interaction of photons with metallic nanostructures can confine electromagnetic fields to a subwavelength volume, enabling light matter interactions with unprecedented resolution. Based on this concept, researchers have developed near-field optical nanotweezers[2,3] and nanoscale plasmonic motors[4,5] that demonstrate the non-invasive manipulation of individual nano-objects with light.

While these applications are fundamental to nanotechnology, they all are based on weak light-matter interactions and are therefore limited to the generation of relatively low magnitude pressure and forces, typically in the ~100 Pa and pN regimes (1 pN = 10^{-12} Newton)[6]. On the other hand, the standard diamond anvil cell technique for high-pressure studies reaches extreme pressure values of ~600 GPa[7], but it is however limited to micro-scale resolution. The ability to efficiently generate and control high pressure stimulus at the nanoscale would be transformative to variety of applications that demand strong mechanical interactions, including the investigation of cell biomechanics[8]. Most importantly, it can benefit fields of enormous interest for fundamental physics and chemistry, such as exploration of molecular and biomolecular materials response to extreme thermodynamic conditions[9–12]. For instance, exotic phase transitions, altered vibrational dynamics, and modified excited electronic states all typically occur in the range of~100 GPa, and need precise nanoscale control of pressure generation to be studied efficiently at the single-molecule level.

This regime of high pressure can be obtained by leveraging non-linear interaction of high intensity ultra-short laser pulses

[a]Laser Processing and Plasmonics Laboratory, Department of Engineering Physics, Polytechnique Montréal, Montréal, Québec H3C 3A7, Canada
[b]SUPA, School of Physics and Astronomy, University of St. Andrews, North Haugh, St. Andrews, KY16 9SS, UK
[c]Dipartimento di Chimica "A.M. Tamburro", Università della Basilicata, Viadell'Ateneo Lucano 10, 85100 Potenza, Italy
[d]Laboratory of Biosensors and Nanomachines, Department of Chemistry, Université de Montréal, Montréal, Québec, H3T 1J4, Canada
[†]Electronic supplementary information (ESI) available: Spectroscopic characterization of individual AuBT. Schematic of the time-resolved shadowgraphic experimental setup. Precisions on the calculation of the AuBT displacement post irradiation. Correlation between SEM characterization data and nanobubble detection data obtained from individual AuBTs. The used ITO optical properties and other computational details.

DOI: 10.1039/C6NR03888C

with metallic nanostructures, which is known to lead to extremely confined, plasmon-enhanced energy deposition in the near field[13]. Using gold nanospheres and nanorods, this type of non-linear interaction has been shown to induce the controlled nanoablation of surfaces[14,15], as well as optical breakdown and production of nanoscale bubbles[16–18] in aqueous environment, with pressures reaching values of ~100 GPa. However, these systems lack the stability and uniformity required for reliable stress induction. In addition, nanospheres are highly symmetrical structures with a limited number of optically active plasmon modes, which restrain the diversity of configurations, patterns and conditions in which mechanical stress can be generated.

In this work, we demonstrate a platform to control pressure stimulation at the nanoscale that is based on an array of plasmonic gold bowtie (AuBT) nano-antennas[19]. This platform uses AuBT to confine electromagnetic fields to a nano-sized gap between the two plasmonic nano-triangles, creating very large field enhancement. Similar platforms have been previously used for a variety of applications demanding precise control of intense fields, including high-harmonic generation[20], nanoscale optical trapping[2] and single molecule fluorescence enhancement[21]. Importantly, the resonance wavelength and near-field intensity can be engineered by modifying the AuBT gap size, length, thickness and radius of curvature, which provide important tunability for a wide range of the electromagnetic spectra[22,23,24]. In addition, due to their relative asymmetry, AuBT exhibit polarization-dependent plasmon modes that can be exploited to precisely control the spatial distribution of pressure stimulus at the nanoscale. Because of these characteristics, AuBT is a perfect structure for the development of a tunable mechanical stress induction platform.

To demonstrate the utility of this platform, we designed and fabricated a durable AuBT array that maximizes near-field enhancement and non-linear interaction with its environment, and minimizes direct light absorption to avoid thermal damage to the structure. We then investigated the pressure generated by this AuBT array following excitation with polarized near-infrared femtosecond (fs) laser pulses. By tuning the laser fluence, we observed the formation of nanoscale bubbles around the AuBT using time-resolved imaging, which strongly suggest that intense pressure and thermodynamic states are generated by the platform. Scanning Electron Microscopy (SEM) characterization of AuBTs post irradiation revealed a laser fluence threshold beyond which their morphology is modified, showing strongly polarization-dependent attributes. SEM observations and simulation data suggest that these morphological modifications are due to intense pressure in the range of ~1TPa, which was generated in the AuBT near-field, in patterns that depend on the laser polarization and the array geometry. The generation of nanobubbles by the structure was invariably connected to significant damage to the platform, setting an upper limit of ~70 mJ/cm^2 for sustainable use. Our simulation data however suggest that pressures in the ~100 GPa regime can still be generated by the AuBT array at laser fluence (30 mJ/cm^2) well below the damage threshold, suggesting that this platform could be used as an efficient and durable extreme pressure stimulator at the nanoscale.

Results and Discussion

Design of the gold bowtie nano-antenna array

We targeted an AuBT array that can efficiently generate high pressure stimuli while avoiding damaging the antenna for a sufficient laser fluence processing window. First, we designed a periodic array of gold nano-triangle dimers on top of an indium tin oxide (ITO) layer, immersed in water, which is intended to be irradiated from the top with a linearly polarized laser beam (Figure 1a). The periodicity of the structure was set to 5 µm in both longitudinal and transversal axes to avoid plasmon coupling between individual dimers. In accordance with our fabrication constraints (see Methods), the thicknesses of the ITO layer and glass substrate were fixed to 100 nm and 1 mm, respectively. The thickness of the gold layer was fixed to 50 nm, which is a reasonable value to attain 20 nm fabrication resolution with electron beam lithography (EBL). Note that since we apply normal incidence laser excitation, the lateral and not the vertical dimension of the AuBT is important for obtaining the desired optical properties. The radii of curvature of the nano-triangle vertexes were evaluated from representative SEM images of fabricated AuBT samples, yielding a typical radius of 20 nm.

Then, we used computational electromagnetic calculations to optimize the design, namely the edge length of the two equilateral nano-triangles forming the bowtie antenna (L: 60 nm - 220 nm) and their separation distance (G: 10 nm - 60 nm). The objective of this optimization process is to (i) minimize the absorption cross-section to avoid thermal damage (ii) maximize the near-field enhancement to enhance non-linear interaction with water molecules and pressure generation and (iii) keep our design within the limits of reliable fabrication. This optimization process is not trivial, due to the intricate dependence of the optical properties on the geometry of the AuBT. For instance, reducing the gap size (G) increases near-field enhancement (Figure 1b), but on the other hand increases the fabrication complexity and absorption cross-section for 0 < L < ~115 nm (Figure 1c).

Based on the mapping of the absorption cross-section and near-field enhancement in function of the design parameters (L and G), we selected a specific AuBT geometry that meets all design constraints. This geometry (G = 20 nm, L = 100 nm) yields a relatively low absorption cross-section ($C_{abs,G=20,L=100}$ = 16700 nm^2) and a relatively high maximal near-field enhancement ($|E|/|E_0|$ = 23.0 at 800 nm). The AuBT flare angle (as defined in Figure 1a) was fixed to φ=60° as this value represents a good compromise based on our optimization criteria (Figure S1). This nanostructure in addition exhibits a strongly polarization-dependent near-field distribution (Figure 1d-f), as illustrated by their mapping for three different polarizations (longitudinal (LP), diagonal (DP) and transversal (TP)), which shows unique

View Article Online
DOI: 10.1039/C6NR03888C

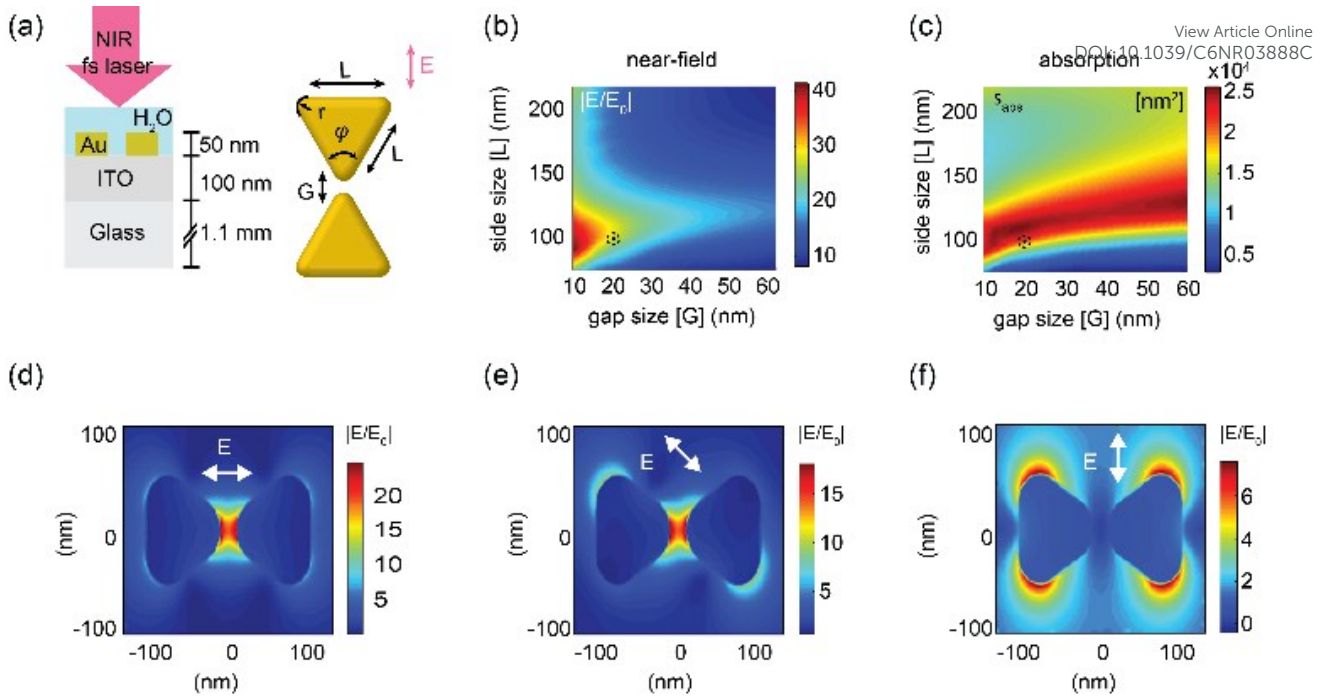

FIGURE 1 Designing a AuBT array for efficient pressure and bubble generation. (a) Cross-section and top view of the AuBT structure used in the modelling. Irradiation was applied from the top in water environment. The radii of curvature was fixed to r = 20 nm, while the edge length (L) and the gap distance (G) were variables in the design study. The flare angle (φ) was fixed at 60 degrees. (b) Maximum near-field enhancement at mid-height and (c) AuBT absorption cross-section as a function of G and L for LP excitation. The black dot indicates the selected geometry. Figures (d), (e) and (f) represent the calculated near-field enhancement at mid-height for three different polarizations for G = 20 nm and L = 100 nm.

geometrical features, and maximal field enhancement varying from 23.0 (LP) to 17.9 (DP) and 6.8 (TP).

We fabricated the AuBT arrays on transparent glass substrates using electron beam lithography (EBL) (see Methods). Briefly, a standard lift-off nanofabrication process was performed using a positive resist (polymethyl methacrylate (PMMA)) and commercial ITO coated glass substrates. Figure 2a shows dark-field optical microscopy images of a typical 20x20 AuBT array. The fabricated platform reproduced the design accurately, resulting in slight differences between the targeted and fabricated geometries, less than 3% and 10% for the AuBT length (L) and gap (G), respectively (Figure 2b).

The coupling plasmonic behaviour of the AuBTs was verified by optical characterization. Non polarization-resolved spectra of individual AuBTs immersed in water were obtained using dark-field microscopy, showing the existence of two peaks at 716 nm and 770 nm, which correspond to the transverse nano-

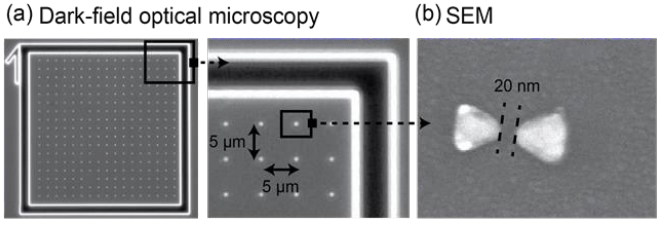

FIGURE 2 (a) Dark-field optical microscopy images of a typical 20 x 20 AuBT array fabricated by electron beam lithography (L = 100 ± 3 nm and G = 20 ± 2 nm). Each AuBT array is enclosed in a numbered square gold frame. (b) SEM picture of an individual AuBT.

triangle resonance mode and the coupled longitudinal AuBT resonance mode, respectively (Figure S2). These results indicated the plasmonic behaviour of the AuBT, in agreement with simulation predictions.

Generation and detection of arrays of nanobubbles

Pressure stress at the nanoscale is challenging to measure directly. While piezo-resistive sensors[25] and hydrophones[26] can be used to directly measure pressure waves generated in confined area, they do not offer the necessary resolution to reliably measure pressure in nano-sized volumes.

One of the most striking effects of stress generation in a liquid environment is cavitation, i.e. the formation of bubbles due to intense thermo-mechanical stress that ruptures the hydrogen bonds network between water molecules[27]. Moreover, bubble collapse may also result in intense pressure stress and shock waves emission, and therefore act as a secondary source of localized pressure generation[28,29]. Water cavitation around laser-irradiated plasmonic nanoparticles has been intensively studied in the past few years[18,30–32], and extensively used in the context of cell nanosurgery[33]. Recently, cavitation resulting from the interaction of ultrashort laser pulses with plasmonic nanospheres[16,18,31] and nanorods[17] have been associated to the excitation of nanoplasmas in the plasmon-enhanced near-field around the nanoparticles, which provides a mechanism by which our platform should generate strong pressure waves.

To test the ability of the AuBT platform to generate intense mechanical stress and pressure at the nanoscale, we therefore

View Article Online
DOI: 10.1039/C6NR03888C

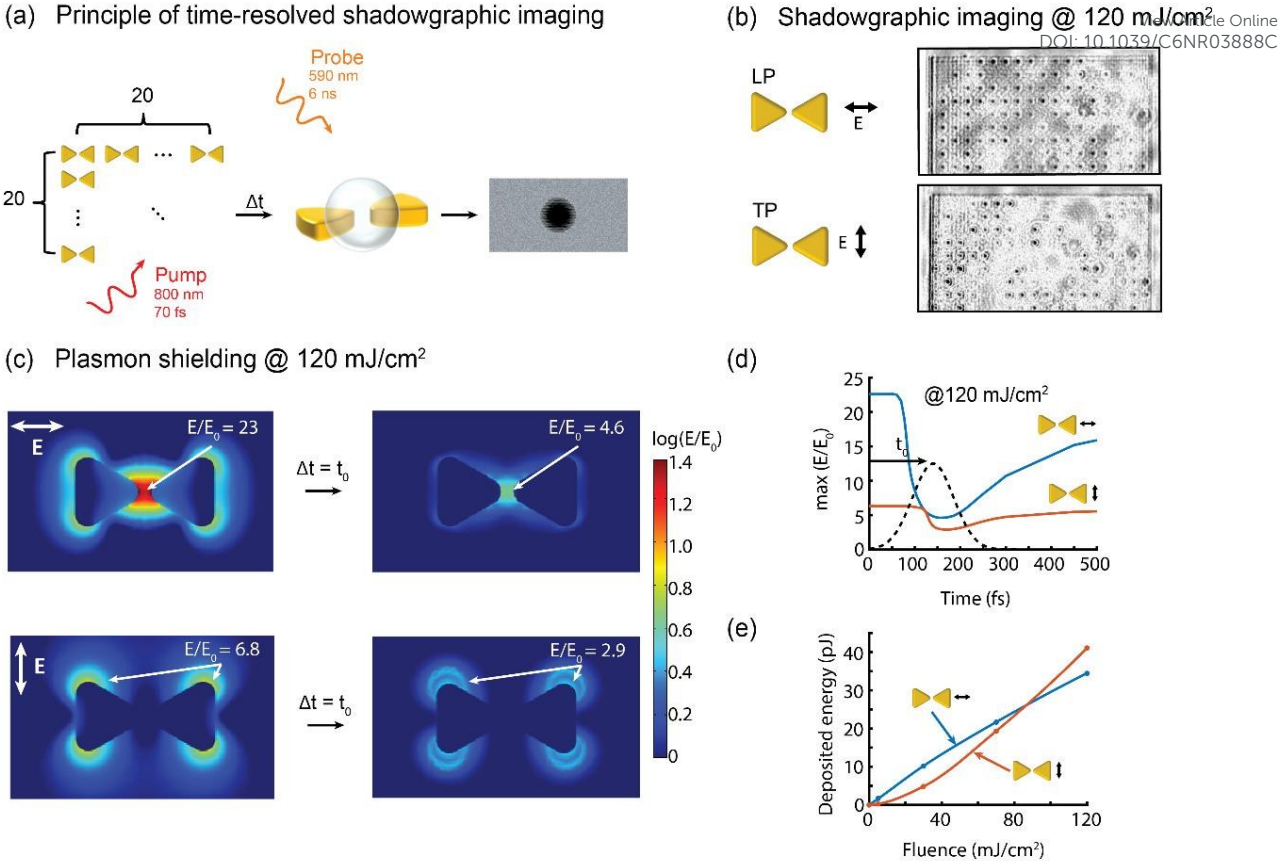

FIGURE 3 Principle of time-resolved shadowgraphic imaging. The sample is a 20 x 20 array of AuBT (periodicity: 5 µm). (b) Arrays of nanobubbles generated by fs laser irradiation with LP and TP polarizations. Bubbles were detected 15 ns after their generation. (laser fluence 120 mJ/cm²) (c) Simulated field enhancement distribution for LP (top) and LT (bottom) polarizations at t=0 and t=t_0, corresponding to the peak incident intensity. Field enhancement is shown at the nano-triangle mid-height plane. (laser fluence 120 mJ/cm²) (d) Simulated time-evolution of the maximal near-field enhancement for LP and TP polarizations. The dashed line shows the fs laser pulse. (laser fluence 120 mJ/cm²) (e) Total energy deposited in the system as a function of the laser fluence for LP and TP excitation.

investigated the generation of nanobubbles in the plasmon-enhanced near-field around the structure. Because the typical lifetime of a nanobubble is under ~100 ns, conventional imaging techniques and commercial cameras cannot be used for their reliable detection. Therefore, we employed a time-resolved shadowgraphic imaging technique that enables direct detection and measurement of transient nanometer-sized bubbles with a spatial and time resolution of ~600 nm and ~ 1 ns, respectively (see Methods and Figure S3). Figure 3a shows a schematic representation of the AuBT platform and the working principle of the time-resolved shadowgraphic imaging. Arrays of nanobubbles were generated and detected following the excitation of the AuBT with a single ultrashort laser pulse (800 nm, 70 fs) for LP and TP polarizations (Figures 3b). Nanobubbles were detected 15 ns after their generation.

The threshold for cavitation was evaluated to be ~70mJ/cm², regardless of the laser beam polarization (LP or TP). This result is surprising given the predicted near-field enhancement around the AuBT, which was previously shown to be highly dependent on the laser polarization (Figures 2d-f). To explain this apparent discrepancy, we analyzed the AuBT antenna using a finite-element based model that simulate the interaction of ultrashort laser pulses with plasmonic nanostructures in water.[16,17] (see Methods). Briefly, in addition to the linear absorption of photons by the plasmonic nanostructure, this model simulates the non-linear interaction of plasmon-enhanced strong electromagnetic fields with surrounding water molecules, and the possible excitation of nanoscale plasmas as an extra channel for energy deposition into the system.

Simulation results suggest that this model can explain the vanishing difference of cavitation threshold between LP and TP polarizations. Indeed, our results show that plasmon modes and near-field intensity are heavily modified by a nanoplasma generated around the AuBT during the pulse, a phenomenon known as “plasmon shielding”[17]. Our model accounts for the time-dependent permittivity of the AuBT surrounding medium, enabling the calculation of a time-dependent near-field and absorption cross section (see SI). For instance, at a fluence of 120 mJ/cm², our simulation results show that the maximal field enhancement is being reduced from 23 to 4.6 and from 6.8 to 2.9 at a time corresponding to the peak of laser intensity for the LP and TP polarizations, respectively (Figures 3c and 3d). A similar effect is observed on the time-dependent AuBT absorption cross-section, being reduced from 16700 nm² to 2100 nm² and from 6900 nm² to 3800 nm² for the LP and TP polarizations, respectively (Figure S4). Plasmon shielding strongly influence the amount of energy deposited in the water

View Article Online
DOI: 10.1039/C6NR03888C

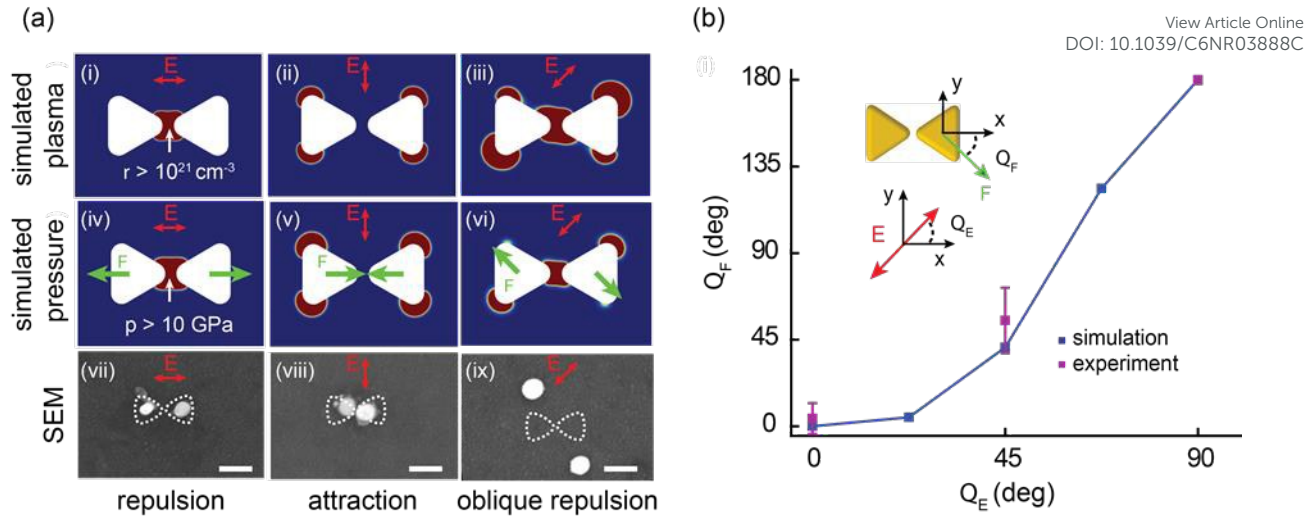

FIGURE 4 Polarization-dependent generation of pressure stimuli following fs laser excitation of AuBT. (a) (i-iii) Nano-plasma simulations at 120 mJ/cm^2. The red areas indicate regions where the electronic density reaches the optical breakdown threshold in water (ρ >10^{21} cm^{-3}) at the pulse maximum. (iv-vi) Isochoric pressure reached in water after irradiation at 120 mJ/cm^2. The red area shows the region where pressure is larger than 10 GPa. The green arrows indicate the equivalent force acting on the nano-triangle center of mass. Torque is not shown. (vii-ix) SEM pictures showing polarization-depended alteration of AuBT morphology at 120mJ/cm^2. Scale bars correspond to 100 nm. (b) Simulated force direction acting to the nano-triangle center of mass for various polarizations (blue line). Experimentally observed displacement of the nano-triangle due to the polarization-controlled directional pressure stimuli (purple squares). The error bar corresponds to the standard deviation of 4 measurements.

molecules, and thus the bubble nucleation (Figure 3e). In particular, near the cavitation threshold (~70 mJ/cm^2), our simulation suggests that the deposited energy is only weakly dependent on laser polarization, in agreement with experimental observations. These results therefore demonstrate that intense pressure waves and extreme thermodynamic states are generated as a result of the laser interaction with the AuBT arrays, and strongly suggest that these states are produced by the non-linear excitation of a nanoplasma in the AuBT plasmon-enhanced near-field.

Generation of extreme pressure stimuli with controlled spatial localization

While the presence of large mechanical stress can be deduced from the presence of nanoscale bubbles, the magnitude of the pressure reached in the near-field cannot be directly measured. In addition, time-resolved imaging does not provide sufficient resolution to investigate localization of high pressure in discrete AuBT near-filed regimes spaced ~100 nm apart. Some indirect method must therefore be designed to infer the nanoscale localization of the high-pressure, which is expected considering the distribution of the near-field. Using the finite-element based model discussed previously, we discovered that the excitation of plasma and generation of pressure in the plasmon-enhanced near-field should result in a net force on the AuBT nano-triangles with a well-defined orientation determined by the incident laser polarization (Figure 4a and b, Figure S5). At sufficient fluences, this force should impact the morphology of damaged AuBTs, providing an opportunity to infer the presence of highly localized high-pressure locus in the system from simple SEM measurements.

To demonstrate this, the morphology of individual damaged AuBT was thoroughly investigated using SEM, following irradiation at 120 mJ/cm^2. In agreement with simulations, we observed that the individual triangles that form the AuBT structure are moved on the surface, with an angle that varies with the incident laser polarization (Figure 4a, bottom row). While laser induced gold nano-triangle morphological alteration (i.e., melting) has been previously observed when hexagonally ordered nanostructures were irradiated with either ns[34] or fs[35] laser pulses in air, no directional displacement of the melted gold was ever observed. In our case, the rapid and localized heating of water molecules in the near-field generate pressure that provide an impulse to the nano-triangles, resulting in a displacement with a direction (Figure 4b) and amplitude (see SI, Figure S5) in good agreement with simulations. These results thus strongly suggest that the observed morphological changes are direct consequences of the highly localized pressurized regions in the liquid environment that surrounds the antenna.

The interaction of the AuBT with laser pulses of relatively high fluences (~120 mJ/cm^2) provided a unique, experimentally measurable signature of the localized pressure generation at the nanoscale and validated our model. However, for some applications, especially in cell stimulation studies, the damage of the platform shall be avoided. In this context, we experimentally investigated the AuBT damage process to identify a safe pressure generation operating window for our platform.

We performed thorough correlation of SEM morphology and time-resolved nanobubble images of individual AuBTs. The results showed that the AuBT damage was invariably correlated with the observation of nanobubbles (see SI and Figure S6) and revealed that the AuBT remained intact when irradiated below cavitation threshold (70 mJ/cm^2). The pressure that can be

View Article Online
DOI: 10.1039/C6NR03888C

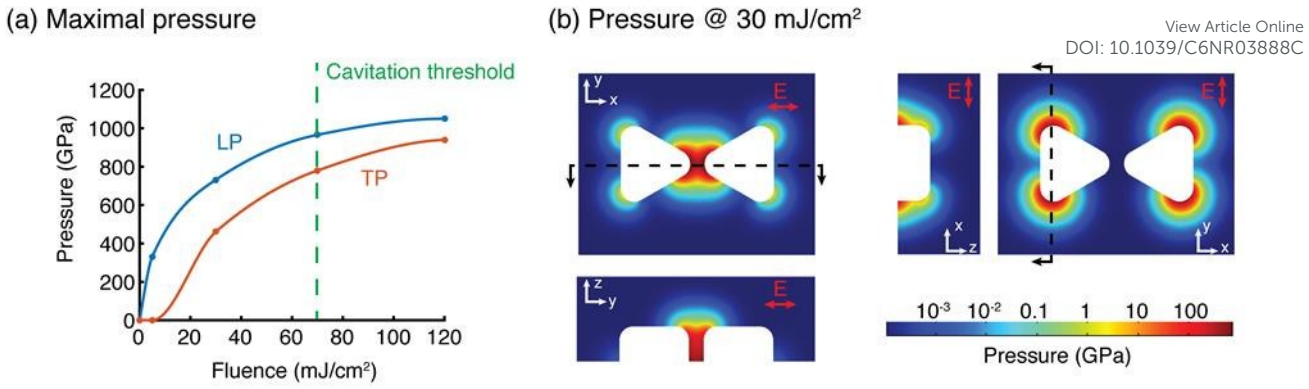

FIGURE 5 (a) Simulation of the maximal isochoric pressure reached in water 2 ps after laser irradiation for TP (blue) and LP (orange) polarizations. The fluence corresponding to the experimental cavitation threshold is shown. (b) Top view and cross-sections of the of the isochoric pressure distribution reached around the AuBT antenna, 2 ps after irradiation at 30 mJ/cm2 for LP (left) and TP (right) polarizations.

generated at these low fluences is challenging to measure, but can be estimated from our finite-element based model. Simulations data suggest that intense pressure waves can still be generated in the near-field (Figure 5a). For instance, excitation at 30 mJ/cm^2, well below the nanobubble generation threshold, should induce pressures with magnitudes of ~700 GPa and ~500 GPa, for LP and TP polarizations, respectively (Figure 5a and b). This initial pressure, maximal at the ITO interface, will decay very rapidly in a few tens of picoseconds as the shockwave propagates in the medium[16].

These results suggest that our platform can generate extreme pressure waves with magnitudes well beyond 100 GPa without damaging the AuBTs. This high-pressure regime reaches the pressure standards of the diamond anvil cell technique[7,12], which is the traditional method for static high-pressure studies at the macro- and micro-scale. Photon-induced generation of sub-TPa pressure in the ps time scale has been previously demonstrated in bulk materials, using standard focusing of ultra-fast laser pulses with high numerical aperture lenses, for nanofabrication[36] (Mazur group) and studies of new material phases[11] (Rode group). Compared to these systems, our plasmonic platform utilizes almost one order of magnitude lower laser pulse energy density and attains one order of magnitude higher localization of the pressure stimulus because of the strong near-field enhancement and confinement of the fs laser irradiation. This platform thus provides a unique, programmable way of generating extreme pressure at specific, light polarization controlled points in nanoscale volumes, which can benefit the exploration of exotic phase transitions and chemical reactions in liquids at the single-molecule level.

Note that when the required spatial resolution for the pressure stimulus is above ~ λ/2, UV photolithography may be used as a more cost and time efficient method to fabricate the platform. However, extreme confinement requires fabrication resolution as low as 20 nm, which can be attained with EBL.

Conclusions

In summary, we demonstrated a new platform made of highly polarisable non-symmetric AuBT that can be excited with linearly polarized light to generate ~100GPa pressure waves at the nanoscale. The generation of mechanical stress in the medium was shown to result from the non-linear photoexcitation of a plasma in the plasmon-enhanced near-field around the nanostructures. Based on the highly polarisable nature of the plasmon modes of non-symmetric AuBT, we demonstrate that tuning the laser polarization can control the magnitude and spatial localization of pressure stimulation. In contrast to heat dissipation driven bubble and pressure generation, optical breakdown driven bubble generation can be extremely confined, and therefore lead to extremely high pressure regimes that cannot be reached with other methods. Based on this principle, sophisticated pressure stimulus like nano-jets and nano-turbulences might in addition be generated by exciting specifically designed non-symmetric nanostructures. This kind of opto-mechanical transducers could be exploited to non-invasively and spatiotemporally probe the mechanical response of cells and single-molecules in time and pressure regimes that remain largely unexplored, with interesting and exciting perspectives for biophysics, physical chemistry and nanotechnology.

Methods

Gold bowtie nano-antenna fabrication and characterization

AuBT were fabricated using electronic beam lithography (EBL). First, PMMA resist was spin coated (4000rpm) on indium tin oxide (ITO) coated glass slides (Sigma-Aldrich, surface resistivity 30-60 Ω/sq, 100 nm thick ITO layer on a 1.1 mm thick glass support). The resulting thickness of PMMA layer was 150 nm and soft baking of the resist was carried out at 170°C for 30 minutes. Then, EBL exposition was performed and followed by sample development in a 1:3 methyl isobutyl ketone solution (in isopropanol) for 105 seconds. Then, the samples were coated with a 2 nm thick Cr (adhesion layer) layer and a 50 nm Au thick layer by evaporation. Sonication of the samples in acetone for 20 minutes was performed in order to wash off the resist and any metal deposited outside of the exposed zone.

The AuBTs were organized in 0.5 mm x 0.5 mm blocks with 5µm periodicity. Each AuBT unit consisted of pairs of 100 ± 3 nm

sized nano-triangles separated by 20 ± 2nm gap. Morphological characterization of the AuBT samples prior and after irradiation was performed using a Field Emission SEM (Hitachi S-4700). Spectroscopic characterization of single AuBT was performed using an inverted microscope (Eclipse Ti-U, Nikon) and non polarization-resolved dark-field excitation. We used a standard halogen lamp (Nikon) and a dark-field condenser (Nikon, 0.95-0.80 NA) for the excitation of the AuBTs, while a 60X objective lens (Nikon, Plan Fluor ELWD) was used to collect the scatting signal. Scattering signals from individual AuBTs were recorded with an imaging spectrograph (Shamrock 550, Andor Technology) equipped with a charge-coupled device detecting camera (Newton 940).

Gold bowtie nano-antenna modelling

The modeling is largely based on a previously published model [15–17]. Electromagnetic field enhancement around AuBT was obtained by solving the Helmoltz equation, considering the complete AuBT geometry, including the ITO and glass layers of the supporting substrate. The electromagnetic field calculation accounts for the variation of the AuBT surrounding medium at every time step, the water permittivity being time-dependent and coupled to the "nanoplasma" calculations (see SI). The electronic and lattice temperatures inside the gold nanostructure were calculated via a parabolic two-temperature model (TTM) based on Boltzmann semi-classical transport equations[37]. Photoexcitation of plasma in the near-field is calculated from the combined effect of impact ionization and strong-field photoionization, following Keldysh theory[38]. Plasma dynamics is described by a set of two diffusion equations using dense plasma theory formalism[39]. Water is heated from conductive heat transfer at the gold-water interface, as well as plasma relaxation and recombination. The time dependent plasma density locally and transiently alters the water electric permittivity, modifying the electromagnetic field in turn. Gold permittivity, scaled for nanometer-sized particles, is taken from ref[40] and is assumed not to vary during the fs irradiation. Water equation of state is taken from the parameterizations of the IAPWS[41] and SESAME[42] in their own domains of validity. Thermodynamic trajectory of water in the state diagram is assumed to be isochoric (constant density) due to the ultrafast nature of the laser interaction and electron-ions coupling (~1-3 ps), which is much faster than the water molecules collision time (few ps[43]). The pressure was calculated using the SESAME[41] and IAPWS[42] equations of state and is a function of the temperature only, since the water density is assumed to be constant. The force was calculated as the integral of the pressure gradient on the surface. Details on plasma dynamics, TTM, ITO layer optical properties and computational domain can be found in the SI and Figure S7. The equations are solved self-consistently with the finite-elements method, using the commercial software Comsol (Comsol, Inc., Burlington MA).

Gold bowtie nano-antenna excitation and nanobubble detection

The AuBT samples were imaged using a home-made upright microscope equipped with a long working distance 50X objective lens (Mitutoyo, NA = 0.55) and a CCD camera (IMI Teck IMB-17FT). A Ti:Sapphire laser (6 mJ/pulse, 45 fs, 800 nm, 1 kHz, Spitfire from Spectra-Physics) was used for the excitation of the AuBT. The laser beam was first directed to a homogenizer (Focal-piShaper 9_TiS, AdlOptica) and then delivered to the sample level using a convex lens (f = 300 mm) (Figure S3). The AuBT samples were placed on the top of a glass cover slip by using a polydimethylsiloxane (PDMS) O-ring. The gap between the sample and the cover slip was filled with deionised water. A "top-hat" profile was measured (120 µm spot size) at the AuBT sample level. Single shot irradiation was applied with linear polarized light. Time-resolved imaging methodology was employed to study the nanobubbles generated around the AuBT. In particular, nanosecond (ns) pulses (Quantel, 532nm, τ = 6 ns) were used to pump a rhodamine dye placed in a transparent container. The emitted light (broad peak at 590 nm, τ ~ 6 ns) enabled time-resolved shadowgraphic imaging of nanobubbles 15 ns after their generation. More details on the imaging methodology can be found elsewhere[18].

Acknowledgements

CB acknowledges funding from the EU under a Marie Curie Fellowship, FP7-PEOPLE-2013-IOF, project reference 624888. We would like to thank Prof. Ali Hatef from Nipissing University for providing preliminary simulation data of the AuBT optical response and Dr. Sergiy Patskovsky for his assistance on the AuBT spectra characterization.

References

1 D. G. Grier, *Nature*, 2003, **424**, 810–6.
2 J. Berthelot, S. S. Aćimović, M. L. Juan, M. P. Kreuzer, J. Renger and R. Quidant, *Nat. Nanotechnol.*, 2014, **9**, 295–9.
3 J. C. Ndukaife, A. V. Kildishev, A. G. A. Nnanna, V. M. Shalaev, S. T. Wereley and A. Boltasseva, *Nat. Nanotechnol.*, 2015, **11**, 53–59.
4 M. Liu, T. Zentgraf, Y. Liu, G. Bartal and X. Zhang, *Nat. Nanotechnol.*, 2010, **5**, 570–573.
5 L. Shao, Z. J. Yang, D. Andrén, P. Johansson and M. Käll, *ACS Nano*, 2015, **9**, 12542–12551.
6 M. Dienerowitz, *J. Nanophotonics*, 2008, **2**, 021875.
7 L. Dubrovinsky, N. Dubrovinskaia, V. B. Prakapenka and A. M. Abakumov, *Nat. Commun.*, 2012, **3**, 1163.
8 K. Haase, A. E. Pelling and K. Haase, *J. R. Soc. Interface*, 2015, **12**, 20140970.
9 R. J. Hemley, *Annu. Rev. Phys. Chem.*, 2000, **51**, 763–800.
10 Y. Fu and D. D. Dlott, *J. Phys. Chem. C*, 2015, **119**, 6373–6381.
11 L. Rapp, B. Haberl, C. J. Pickard, J. E. Bradby, E. G. Gamaly, J. S. Williams and A. V Rode, *Nat. Commun.*, 2015, **6**, 7555.
12 P. Dalladay-Simpson, R. T. Howie and E. Gregoryanz, *Nature*, 2016, **529**, 63–67.
13 A. Plech, V. Kotaidis, M. Lorenc and J. Boneberg, *Nat. Phys.*, 2005, **2**, 44–47.
14 D. Eversole, B. Luk'yanchuk and A. Ben-Yakar, *Appl. Phys. A*, 2007, **89**, 283–291.

15 A. Robitaille, E. Boulais and M. Meunier, *Opt. Express*, 2013, **21**, 9703–10.
16 E. Boulais, R. Lachaine and M. Meunier, *Nano Lett.*, 2012, **12**, 4763–9.
17 E. Boulais, R. Lachaine and M. Meunier, *J. Phys. Chem. C*, 2013.
18 C. Boutopoulos, A. Hatef, M. Fortin-Deschênes and M. Meunier, *Nanoscale*, 2015, **7**, 11758–11765.
19 D. P. Fromm, A. Sundaramurthy, P. James Schuck, G. Kino and W. E. Moerner, *Nano Lett.*, 2004, **4**, 957–961.
20 S. Kim, J. Jin, Y.-J. Kim, I.-Y. Park, Y. Kim and S.-W. Kim, *Nature*, 2008, **453**, 757–760.
21 A. Kinkhabwala, Z. Yu, S. Fan, Y. Avlasevich, K. Müllen and W. E. Moerner, *Nat. Photonics*, 2009, **3**, 654–657.
22 D. A. Rosen and A. R. Tao, *ACS Appl. Mater. Interfaces*, 2014, **6**, 4134–4142.
23 M. Kaniber, K. Schraml, A. Regler, J. Bartl, G. Glashagen, F. Flassig, J. Wierzbowski and J. J. Finley, *Sci. Rep.*, 2016, **6**, 23203.
24 X. Zhang, C. Chung, S. Wang, H. Subbaraman, Z. Pan, Q. Zhan and R. T. Chen, *IEEE Antennas Wirel. Propag. Lett.*, 2016, **15**, 1377–1381.
25 M. Li, H. X. Tang and M. L. Roukes, *Nat. Nanotechnol.*, 2007, **2**, 114–20.
26 A. Arvengas, K. Davitt and F. Caupin, *Rev. Sci. Instrum.*, 2011, **82**, 034904.
27 Christopher E. Brennen, *Cavitation and Bubble Dynamics*, Oxford University Press, New York, 1995, vol. 4.
28 E.-A. Brujan and A. Vogel, *J. Fluid Mech.*, 2006, **558**, 281.
29 W. Lauterborn and A. Vogel, *Bubble Dynamics and Shock Waves*, Springer Berlin Heidelberg, Berlin, Heidelberg, 2013.
30 D. Lapotko, *Opt. Express*, 2009, **17**, 2538–56.
31 R. Lachaine, E. Boulais and M. Meunier, *ACS Photonics*, 2014, **1**, 331–336.
32 E.-A. Brujan, *Microfluid. Nanofluidics*, 2011, **11**, 511–517.
33 E. Boulais, R. Lachaine, A. Hatef and M. Meunier, *J. Photochem. Photobiol. C Photochem. Rev.*, 2013, **17**, 26–49.
34 R. Morarescu, D. B. Sánchez, N. Borg, T. A. Vartanyan, F. Träger and F. Hubenthal, *Appl. Surf. Sci.*, 2009, **255**, 9822–9825.
35 S. Dickreuter, J. Gleixner, A. Kolloch, J. Boneberg, E. Scheer and P. Leiderer, *Beilstein J. Nanotechnol.*, 2013, **4**, 588–602.
36 E. N. Glezer and E. Mazur, *Appl. Phys. Lett.*, 1997, **71**, 882.
37 N. Singh, *Int. J. Mod. Phys. B*, 2010, **24**, 1141–1158.
38 A. Vogel, J. Noack, G. Hüttman and G. Paltauf, *Appl. Phys. B*, 2005, **81**, 1015–1047.
39 L. Hallo, A. Bourgeade, V. T. Tikhonchuk, C. Mezel and J. Breil, *Phys. Rev. B - Condens. Matter Mater. Phys.*, 2007, **76**, 1–12.
40 P. B. Johnson and R. W. Christry, *Phys. Rev. B*, 1972, **6**, 4370–4379.
41 W. Wagner and A. Pruß, *J. Phys. Chem. Ref. Data*, 1999, **31**, 387.
42 SESAME: The Los Alamos National Laboratory Equation-of-State Database, Report No. ucrl-7118 and ucrl-52190; Lyon, S. P., Johnson, J. D., Eds.; Los Alamos National Laboratory: Los Alamos, NM, 1979. The water table used here was SESAME table 7150.
43 B. C. Garrett, D. A. Dixon, D. M. Camaioni, D. M. Chipman, M. A. Johnson, C. D. Jonah, G. A. Kimmel, J. H. Miller, T. N. Rescigno, P. J. Rossky, S. S. Xantheas, S. D. Colson, A. H. Laufer, D. Ray, P. F. Barbara, D. M. Bartels, K. H. Becker, K. H. Bowen, S. E. Bradforth, I. Carmichael, J. V. Coe, L. R. Corrales, J. P. Cowin, M. Dupuis, K. B. Eisenthal, J. A. Franz, M. S. Gutowski, K. D. Jordan, B. D. Kay, J. A. LaVerne, S. V. Lymar, T. E. Madey, C. W. McCurdy, D. Meisel, S. Mukamel, A. R. Nilsson, T. M. Orlando, N. G. Petrik, S. M. Pimblott, J. R. Rustad, G. K. Schenter, S. J. Singer, A. Tokmakoff, L. S. Wang, C. Wittig and T. S. Zwier, *Chem. Rev.*, 2005, **105**, 355–389.